Journal of Applied Physics

RESEARCH ARTICLE | JULY 31 2023

Effect of iron thicknesses on spin transport in a Fe/Au bilayer system

J. Briones ; M. Weber ; B. Stadtmüller ; H. C. Schneider ; B. Rethfeld

J. Appl. Phys. 134, 043907 (2023)
https://doi.org/10.1063/5.0148731

AIP Publishing

Journal of Applied Physics ARTICLE pubs.aip.org/aip/jap

Effect of iron thicknesses on spin transport in a Fe/Au bilayer system

Cite as: J. Appl. Phys. **134**, 043907 (2023); doi: 10.1063/5.0148731
Submitted: 2 March 2023 · Accepted: 4 July 2023 ·
Published Online: 31 July 2023

J. Briones,[1,a)] M. Weber,[1] B. Stadtmüller,[1,2] H. C. Schneider,[1] and B. Rethfeld[1]

AFFILIATIONS

[1]Department of Physics and OPTIMAS Research Center, RPTU Kaiserslautern-Landau, Gottlieb-Daimler-Str. 76, 67663 Kaiserslautern, Germany
[2]Institute of Physics, Johannes Gutenberg University Mainz, 55128 Mainz, Germany

[a)]**Author to whom correspondence should be addressed:** rethfeld@physik.uni-kl.de

ABSTRACT

This paper is concerned with a theoretical analysis of the behavior of optically excited spin currents in bilayer and multilayer systems of ferromagnetic and normal metals. As the propagation, control, and manipulation of the spin currents created in ferromagnets by femtosecond optical pulses is of particular interest, we examine the influence of different thicknesses of the constituent layers for the case of electrons excited several electronvolts above the Fermi level. Using a Monte-Carlo simulation framework for such highly excited electrons, we first examine the spatiotemporal characteristics of the spin current density driven in a Fe layer, where the absorption profile of the light pulse plays an important role. Further, we examine how the combination of light absorption profile, spin-dependent transmission probabilities, and iron layer thickness affects spin current density in a Fe/Au bilayer system. For high-energy electrons studied here, the interface and secondary electron generation have a small influence on spin transport in the bilayer system. However, we find that spin injection from one layer to another is most effective within a certain range of iron layer thicknesses.

I. INTRODUCTION

In the race to reduce power consumption and increase processing capability, the use of spin rather than charge promises a new generation of microelectronics. Spintronics based on metallic multilayers employs these structures for data storage and spin transport for information exchange. Conventional spintronics employs spin currents and spin densities that are due to non-equilibrium electrons that are still close to the Fermi energy.[1]

Even though metal-based spintronics is a very well established field, it continues to rapidly evolve. Among the current goals of spintronics research are the manipulation of spin ensembles carried by electrons that are energetically farther away from the Fermi energy. For non-equilibrium electrons in general, scattering events determine the electronic transport in magnetic materials, regardless of the source that drives the currents, for instance, electrical spin injection from magnetic (metallic or semiconductor) electrodes,[2–4] or manipulating spin polarization by alternating-current (AC) magnetic fields via Zeeman interaction,[5,6] to name but a few. If one considers electron injection at high energies or, in particular, optical excitation of electronics, dynamics with an essential electronic energy dependence and its interplay with spin transport becomes more important. For this hot-electron spin transport, an intermediate "superdiffusive" regime was identified,[7] which has characteristics somewhat different from ballistic and diffusive transport. Based on experimental evidence,[8,9] it is believed that superdiffusive spin currents can be launched from a ferromagnetic layer into adjacent metallic layers and can contribute to the transfer of spin angular momentum that is needed in the ultrafast demagnetization of ferromagnets. An alternative method to describe superdiffusive spin currents is provided by a particle in-cell approach.[10,11] This method to solve the spin-dependent Boltzmann equation can be relatively easily adapted to *ab initio* input.

In this work, we focus on the dynamics and transport of electrons created far away from the Fermi energy by fs laser irradiation. We study a prototypical Fe/Au bilayer system, where optical pulses, which drive the hot-electron spin currents, are absorbed in both the ferromagnetic and normal metal layers. Our approach is based on the Monte-Carlo model for spin-dependent electron dynamics

developed in Ref. 12. In addition to the effects of different collision processes, such as secondary electron generation and elastic scattering, we investigate the influence of different thicknesses of the magnetic layer and the interface transmissions with the intent to understand and optimize spin currents in the structure.

II. THEORETICAL APPROACH

The aim of our study is to predict how different interactions influence the nonequilibrium dynamics and spin injection in FM/M bilayer systems. In our approach, we consider free electron states above E_F as essentially free and focus on the influence of high-energy electrons in spin transport. This section presents the algorithms, equations, and set of parameters that will be used for the simulations presented in this paper.

A. Monte-Carlo method

The asymptotic Monte-Carlo trajectory method[13] is a statistical technique that models binary collision interactions by sampling several trajectories until an estimate of the possible outcomes is obtained. Probability theory is used to implement an algorithm for random sampling of variable x. In probability theory, all possible events $p(x)$ are integrated into a variable referred to as the cumulative distribution function (CDF) $F(x)$ in order to construct a formula that can be used to obtain a value for the variable x.[14] A more thorough and accurate description of how the Monte-Carlo method is done can be found in the literature.[15–17] Here, we will study the dynamics of excited particles using the same technique explained in our previous work.[12] During the simulation, any electron interaction process is treated by random sampling. The time between two successive collisions (time of free flight) τ can be sampled with the random variable $R \in [0, 1]$ as

$$\tau = -\nu_0^{-1} \log(R), \tag{1}$$

when the scattering rate ν_0 is constant. However, assuming a constant total scattering rate, independent of energy, is a statistical overestimation. To compensate, we introduce a further interaction with an energy-dependent probability, which allows the particle to continue its trajectory unperturbed. For the case of several scattering mechanisms as studied in this work, we perform a random sample of collisions using the probability function $p(x)$, which can be replaced with either the differential cross section $d\sigma/d\Omega$, scattering rates ν, or characteristic times τ.

B. Material parameters

We consider a Fe/Au bilayer material irradiated by a Gaussian-like laser pulse of 6 eV photon energy. The iron layer thickness is finite, but the gold layer thickness is taken to be infinite and the electrons are tracked only in the first 10 nm. The laser irradiates the material from the iron side, as shown in Fig. 1 and the maximum laser pulse irradiation is centered at 0 fs. A boundary condition is considered at the iron surface irradiated by the laser pulse, causing all excited particles approaching the surface to be reflected at the surface of the Fe layer. At the end of the gold layer, we consider an open boundary condition. The initial energy and

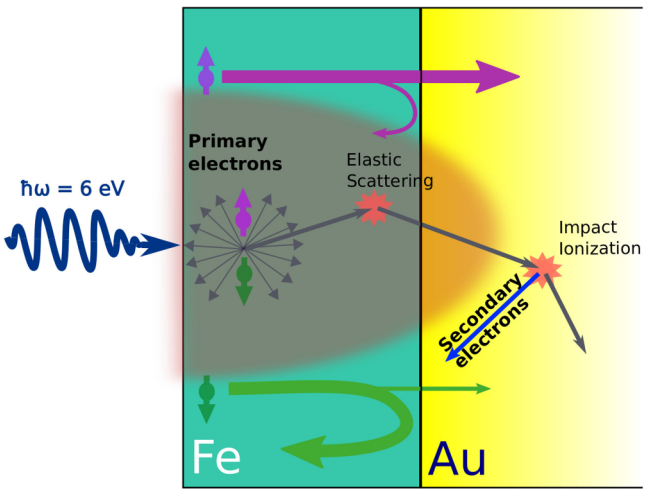

FIG. 1. Schematic representation of the laser irradiation and scattering events in the Fe/Au bilayer system. There are two possible interactions to consider: electron–atom interactions where only the direction of flight changes (elastic scattering) and electron–electron interaction generating secondary electrons (impact ionization). When electrons enter in contact with the interface, their spin determines their transmission probability, and they cross accordingly.

spin distribution of excited electrons is obtained using the same procedure as described in Ref. 12. For states above Fermi energy, we assume a parabolic dispersion relation with the free-electron mass. The virtual minimum of the parabola is located below the Fermi level such that the free electrons with the lowest kinetic energy (i.e., directly above the Fermi level) are moving with Fermi velocity. The initial direction of flight of excited electrons is distributed isotropically. The initial position of the particles must be determined based on the energy of the incident light and the absorption probability of the material depending on its depth, immediately after laser irradiation. As a result of laser irradiation, light intensity in bulk materials follows the Lambert–Beer law, which means the absorbed intensity decreases exponentially with depth. The absorbed intensity of a bilayer system, however, is calculated specifically for this work and depicted in Fig. 5. Excited electrons then interact within the material, either changing only their momentum (elastic scattering) or generating secondary electrons (impact ionization). As soon as an electron reaches the interface, its transmission to the other layer, or its reflection into the same layer, is determined by its spin and generally also its energy.

There are two major parameters for this simulation that we tune and study: (i) The thickness of the Fe layer and (ii) the transmission probability T at the interface. In Ref. 18, transmission probability data from iron to gold have been determined, which is directly applicable to our system. However, our study focuses on the excitation of high-energy electrons where the transmission probability is rather insensitive to the electronic energy (see Fig. 4 in Ref. 18). Thus, we approximate the transmission probability as a constant and also assume it to be independent of the propagation direction of the electrons reaching the interface, i.e., it is assumed

to be identical for electrons traveling from iron to gold and the other way around. The constant transmission probability will be taken from Ref. 18 as $T^{\uparrow} = 0.95$, and $T^{\downarrow} = 0.25$ for spin-up and spin-down electrons, respectively. Note that this procedure effectively includes the influence of the band structure as considered in Ref. 18 into the free-particle approach of highly excited electrons applied in this work.

III. SCATTERING PROCESSES

We trace the dynamics of optically excited electrons by modeling pure jump processes.[17,19,20] As in our first publication in Ref. 12, the photoexcitation of an electron from an occupied band below Fermi energy (E_F) is sampled according to the material's spin-dependent density of states. States above the Fermi energy will be considered as free-electron states with the free-electron mass. Apart from laser excitation, we also consider two kinds of interactions in this study, namely, the electron–atom interaction, which is treated as an elastic scattering process here, and the electron–electron impact ionization, in which energy is transferred to a secondary electron through an inelastic process.

Elastic scattering processes will be modeled as a deflection without transfer of energy. As indicated in Subsection II A, the probability function $p(x)$ will be replaced by the differential cross section based on Mott's cross section in dependence of the scattering angle. We will use $\tau_{el} = 25\,\text{fs}$ as the elastic scattering time,[21] which was applied to study spin transport and spin dynamics in Refs. 10 and 22.

Electron impact ionization is a process in which incident electrons ionize electrons from occupied states into unoccupied states. The newly generated high-energy electrons are referred to as secondary electrons, whereas the optically excited electrons are referred to as primary electrons. With the energy lost by the primary electron of ΔE and the binding energy I of the bound electron, the final energy of the newly ionized electron E_s above Fermi level is $E_s = \Delta E - I$. The amount of transferred energy is assumed to be half of the energy of the incident electron as it was done by Ritchie and Ashley in Ref. 23. They determined the amount of energy transferred to secondary electrons after photo-ionization by using many body perturbation theory. An agreement with experimental results can be found in Ref. 24. For the inelastic scattering rate (τ_{ee}^{-1}), we will consider the energy-dependent collision rate of an excited electron at temperature T_e.[25] Both collision processes and their inclusion are described in more detail in Ref. 12.

IV. RESULTS

The behavior of the nonequilibrium spin transport and spin dynamics will be analyzed in a Fe/Au bilayer system after fs-laser excitation. The laser pulse irradiates the sample from the iron layer (see Fig. 1), and the distance to the interface is measured from this point inwards. Therefore, the thickness of the iron layer will determine the location of the boundary between these materials. Throughout this work, we will use a variety of iron thicknesses, and they will be specified when required. As for the thickness of the gold layer, it is always infinity and we trace the dynamics within the first 10 nm. The effects on the spin transport can be addressed by studying the spin currents generated at the interface of the material. The spin current density j_s is defined as

$$j_s(z, t) \propto q[\langle \eta^{\uparrow} v_{\uparrow} \rangle - \langle \eta^{\downarrow} v_{\downarrow} \rangle], \tag{2}$$

where q is the charge of the electron and $\eta^{\uparrow}$ ($\eta^{\downarrow}$) and $v_{\uparrow}$ ($v_{\downarrow}$) are the particle density and the velocity in direction perpendicular to the irradiated surface for spin up (spin down), respectively. An average over the number of electrons at a specific volume and time is denoted by the angle brackets. Both expressions in Eq. (2) can be separated as

$$J_{up} \propto \langle \eta^{\uparrow} v_{\uparrow} \rangle, \tag{3}$$

$$J_{down} \propto \langle \eta^{\downarrow} v_{\downarrow} \rangle . \tag{4}$$

A. Spin current density in bulk iron

We start by examining the behavior of the spin current density in bulk iron. We then extend the analysis to a more complex system, namely, the Fe/Au bilayer. As it was analyzed in Ref. 12, particles reach an average kinetic energy of less than 2 eV above Fermi level very rapidly because secondary electrons are likely to be generated during the initial time period of the nonequilibrium dynamics.

First, let us focus on the irradiation of bulk iron by femtosecond laser pulses as it was described in Ref. 12. A simulation is performed using a bulk-like Fe film, which is excited by a Gaussian-like fs laser pulse with a photon energy of 6 eV.

As a result of the laser excitation, majority and minority electrons are brought out of equilibrium with different kinetic energy distributions and also random initial directions. We use open boundary conditions at the end of the calculation region of 30 nm thickness, allowing electrons to escape completely from the simulated system.

Figure 2 shows the evolution of the spin current density, as defined by Eq. (2), as a function of time and depth. Note that the magnitude of spin current density remains positive over time and throughout the material. This indicates that, on average, majority of electrons move toward the depth of the material. In addition, the magnitude of spin current density increases steeply with increasing depth and reaches a maximum value at a around 10 nm, which will be analyzed later.

A more detailed observation of the trend in the spin current density is provided in Fig. 3. Here, we depict the contributions to the spin current density in time at different depths, as indicated in Fig. 2. The top graph represents the spin current density j_s for both spin-up (lhs) and spin-down (rhs) electrons, the middle graph depicts the average velocity $\langle v \rangle$, and the bottom graph displays the average particle density $\langle \eta \rangle$, terms used in Eqs. (3) and (4). The color gradient indicates at what depth the variables were selected for analysis. The variables shown in Fig. 3 all seem to exhibit the same behavior in time, but a different maximum value for different depths. We observe again how the average particle density $\langle \eta \rangle$ shows a homogeneous density distribution further in time, which was already discussed in Ref. 12.

Based on these simulations, we have identified two possible causes for this behavior, either the type of scattering or the

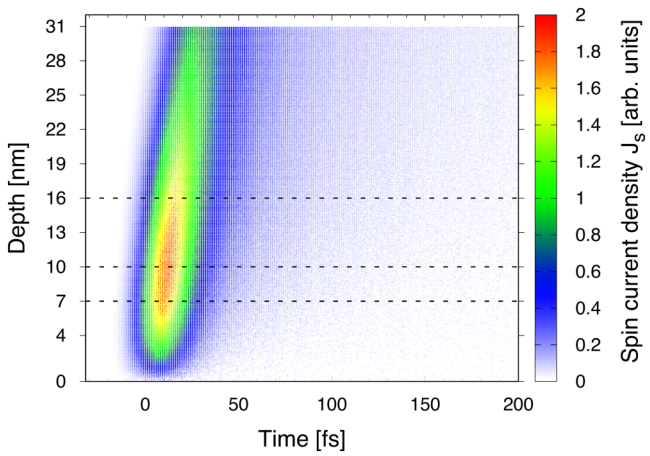

FIG. 2. Development of the spin current density j_s, defined in Eq. (2), in bulk iron over time and in depth, considering secondary electron generation. The dashed lines indicate the position where the spin current density is evaluated further.

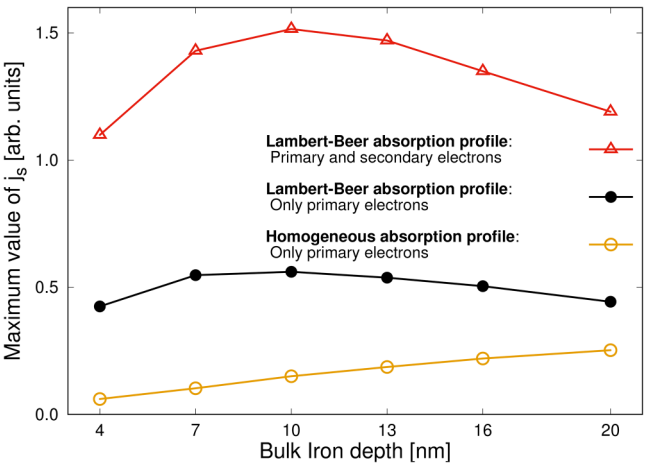

FIG. 4. Maximum values of the spin current density j_s in bulk iron at different depths, for different absorption profiles: Homogeneous absorption profile exciting only primary electrons (yellow curve), Lambert–Beer absorption profile with only primary excitations (black curve), and including primary and secondary electrons (red curve). The values for j_s were obtained using Eq. (2).

absorption profile. In Fig. 4, it is shown how the maximum values of spin current density j_s are affected by the type of scattering and absorption profile. The red curve has been calculated using Lambert–Beer's absorption probability to excite primary electrons and including secondary electron generation. The black curve was done by keeping the same absorption profile, but considering only optically excited electrons. The magnitude of the maximum spin current density j_s in both graphs increases with depth. This increment then slows down until a certain depth (around 10 nm), after which it gradually decreases. These two graphs then differ only qualitatively, which is in agreement with Ref. 12, where it is demonstrated that secondary electrons affect spin current density quantitatively rather than qualitatively. As we consider that the absorption profile influences the observed behavior at different maxima of spin current density, we need to examine the effect of a different profile on primary electrons. This particular scenario involves a homogeneous absorption profile, i.e., there will be the same probability of absorption at every depth.

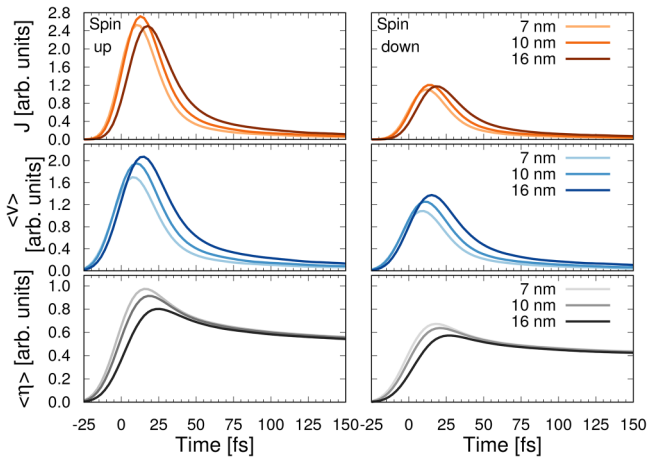

FIG. 3. An analysis of the evolution of the spin-up (lhs) and spin-down (rhs) current density J (top graph), average velocity v, and particle density η in bulk iron, as defined in Eq. (2). The physical quantities are depicted for different depths at the location of the dashed lines in Fig. 2.

As shown in Fig. 4, contrary to other curves, where the maximum values increase until a certain depth, and then gradually decrease (red and black curves), the maximum value of the spin current density j_s in a non-interactive picture (yellow curve), where only elastic scatterings are taking place, increases steadily in depth. This trend can be explained by examining the dynamics of particles following laser absorption. In the non-interactive picture (yellow curve), particles are initially excited based on a constant absorption profile throughout the material. However, as they move toward the depth of the material, the distribution of particles changes since their directionality is initially random. It is likely that particles will move ballistically in the absence of further interactions (change in direction or generation of new particles) and that the density of particles within the material will not be significant. Due to their initial distribution when they are created as well as their interactions with each other, particles, over time, acquire a common directionality through interaction. Hence, the absorption profile is responsible for the observed tendency in the maximum spin current density values in bulk iron at different depths.

B. Spin current density in Fe/Au bilayer systems

We now proceed to examine the spin transport in a bilayer system containing iron and gold. Unlike bulk iron, laser radiation induces primary excitations within both layers in accordance with

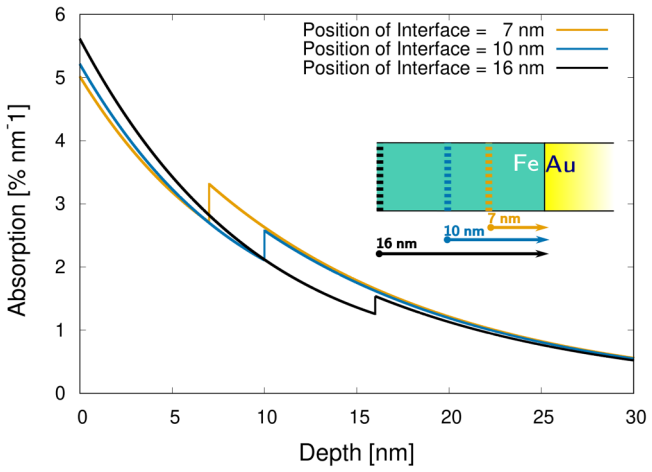

FIG. 5. Absorption probability with respect to the depth for Fe/Au bilayer system with an interface at 7 (yellow), 10 (blue), and 16 nm (black). Both materials have a different absorption profile. At the interface, one can observe a sudden increase in the absorption when the energy enters into the gold layer.

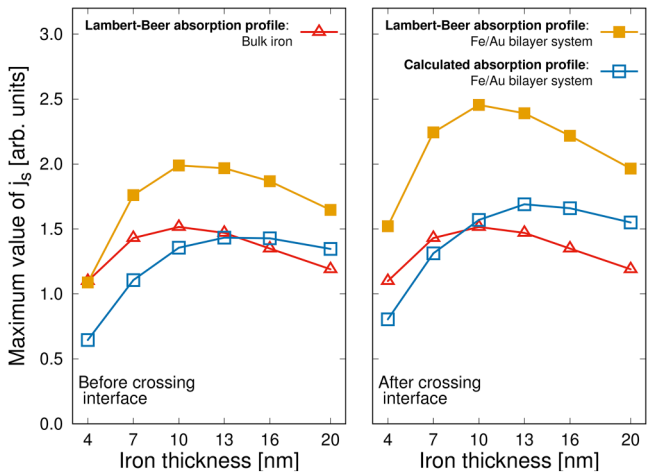

FIG. 6. A comparison of the maximum values of the spin current density j_s, obtained from Eq. (2), for different thicknesses of iron. The value is compared between the Lambert–Beer absorption profile in bulk iron (red) and in the Fe/Au bilayer system (yellow), as well as one simulation using a calculated absorption profile (blue), applying equations from Refs. 26 and 27 and parameters in Ref. 28.

the absorption profile and these are initially distributed within the material accordingly, as illustrated in Fig. 5. Figure 5 shows the data of the laser light absorption probability for different thicknesses of iron layers, which determine the position of the interface in the bilayer system: 7 (yellow curve), 10 (blue curve) and 16 nm (black curve). These curves were obtained following the procedure described in Refs. 26 and 27 with absorption coefficients extracted from Ref. 28. The reason behind choosing these specific sizes is to study how smaller or larger iron layers influence the dynamics. The data in Fig. 5 were calculated for a semi-infinite system, to avoid the reflective effects from gold.

Over time, primary electrons generate secondary electrons, and these subsequently generate further electrons, a process that is repeated in both materials. At the boundary between iron and gold, which will be later addressed as interface, particles are transmitted in different proportion due to the spin-dependent transmission probability (spin filtering effects).

In light of our previous analysis of iron, we now have a better understanding of how the absorption profile influences the behavior of the spin current density. Figure 6 illustrates how the absorption profile and thickness of iron layers affect the maximum value of spin current density in a bilayer system before and after crossing the interface. The magnitude of the peak of the spin current density is compared between the Lambert–Beer absorption profile in bulk iron (red curve), in the Fe/Au bilayer system (yellow curve), and using a calculated absorption profile (blue curve) (using parameters, procedure, and absorption profile from Refs. 26–28, respectively).

In Fig. 6, iron (red) and Fe/Au (yellow) exhibit a large difference in maximum spin-current density as a result of the interface, which increases the value of j_s. However, the interface does not alter the tendency observed over a preferential thickness of iron layer. However, when the calculated absorption profile (from Fig. 5) is taken, the preferred thickness changes and the larger spin current injection from iron to gold appears at a larger iron thickness.

Considering the absolute values of the spin current densities in Fig. 6, we observe two effects: First, an increase of j_s, when we change the calculation from bulk iron (red curves) to the bilayer system (yellow curves). This increase in spin current density can be attributed to the spin-filtering effect of the interface: on the iron side, spin-down electrons are reflected, which reduces the mean velocity $v_\downarrow$ and, therefore, increases j_s according to Eq. (2). On the gold side, the increase of j_s can be directly attributed to the spin-filtered spin-up electrons crossing the interface. When we include the realistic absorption profile depicted in Fig. 5, the absorption and, thus, the number of electrons excited in gold increases. The effect on the spin current density can be observed in Fig. 6 as an overall reduction of the maximum value of the spin current density (see blue curves as compared to yellow curves). The electrons excited in gold with a direction toward the interface are either reflected (spin-down electrons) or transmitted to iron (spin-up electrons). This spin-polarized backflow current leads to a reduction of the spin-filtering effect and, in the case of the calculated absorption profile, even to its compensation.

Spin-dependent particles that cross between layers reconfigure the distribution of particles in gold, which influences the spin current density. This can be analyzed using the equation for spin polarization P,

$$P = \frac{\eta^{\uparrow} - \eta^{\downarrow}}{\eta^{\uparrow} + \eta^{\downarrow}}, \tag{5}$$

where $\eta^{\uparrow}$ ($\eta^{\downarrow}$) is the particle density of spin-up (down) particles.

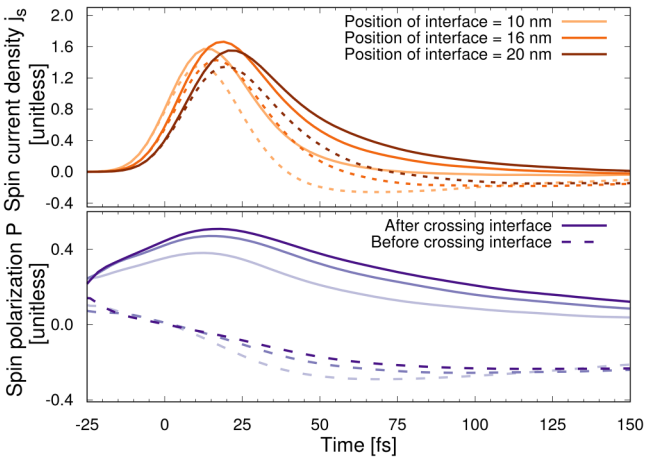

FIG. 7. Spin current density j_s (top graph) and spin polarization P (bottom graph), calculated before (dashed lines) and after (solid lines) crossing the interface. The different thicknesses of the iron layers are displayed as color degraded lines.

Figure 7 shows the spin current density j_s (top graph) and the spin polarization P (lower graph), calculated using Eqs. (2) and (5), respectively, for three different thicknesses of iron layers.

The dashed lines indicate quantities taken before crossing the interface, while the solid lines indicate quantities taken after crossing the interface. The lines depicting the different thicknesses of the iron layer are color degraded. For the spin current density, the observed behavior is similar to that of Fig. 3. In this bilayer system, we focus on the thickness of the iron layer instead of the propagation depth. As shown in Fig. 7, the maximum value of the spin current density j_s increases up to a certain thickness (here 16 nm), but decreases for a thicker film. As a result, it appears that the maximum value of spin current density does not increase with increasing iron layer thickness. Instead, there exists an optimal size of iron layer at which spin injection from iron to gold is more effective. The violet curves in Fig. 7 are the spin polarization curves, which were calculated using Eq. (5). They indicate that in time, always more particles with spin up will cross the interface as a result of the difference in transmission probability for the spins. By increasing the size of the iron layer, the maximum value of spin polarization will be reached at later times. This delay is a consequence of the time necessary for particles to interact within the material and travel toward the interface. As the thickness of the iron layer increases, spin polarization increases since fewer particles crossover to gold when the layer is larger.

V. SUMMARY

In conclusion, we investigated how different iron thicknesses affect the generation of spin currents at the interface of a Fe/Au bilayer system. We first examined the effects of the light absorption profile on the spin current density within a bulk iron layer, and we found that the absorption profile influences the spin current density non-monotonously. For the Fe/Au bilayer, we computed the nonequilibrium transport of excited electrons and studied how different absorption profiles influence the spin current injection from one layer into another. This analysis also revealed that secondary electron generation and the interface affect spin transport only in terms of magnitude. We then investigated the combined effect of light absorption and spin-dependent interface transmission probability on the spin current density in the Fe/Au bilayer system. The magnitude of the spin current density from Fe to Au is influenced by the thickness of the Fe layer and shows a maximum at intermediate thicknesses. We found that the absorption characteristics of the exciting laser pulse has a direct influence on the efficiency of the spin injection from one layer into another.

ACKNOWLEDGMENTS

This study was funded by the Deutsche Forschungsgemeinschaft (DFG, German Research Foundation)—TRR 173/2—268565370 Spin+X (Project B03). B.S. acknowledges financial support by the Dynamics and Topology Center (TopDyn), funded by the State of Rhineland-Palatinate.

AUTHOR DECLARATIONS

Conflict of Interest

The authors have no conflicts to disclose.

Author Contributions

J. Briones: Investigation (equal); Software (lead); Visualization (lead); Writing – original draft (lead); Writing – review & editing (equal). **M. Weber:** Investigation (supporting); Writing – review & editing (equal). **B. Stadtmüller:** Investigation (supporting); Supervision (supporting); Writing – review & editing (supporting). **H. C. Schneider:** Investigation (equal); Supervision (supporting); Writing – review & editing (equal). **B. Rethfeld:** Investigation (equal); Project administration (lead); Supervision (equal); Writing – review & editing (equal).

DATA AVAILABILITY

The data that support the findings of this study are available from the corresponding author upon reasonable request.

REFERENCES

[1]A. Hirohata and K. Takanashi, "Future perspectives for spintronic devices," J. Phys. D: Appl. Phys. **47**, 193001 (2014).
[2]S. Okamoto, "Spin injection and spin transport in paramagnetic insulators," Phys. Rev. B **93**, 064421 (2016).
[3]N. Tombros, C. Jozsa, M. Popinciuc, H. T. Jonkman, and B. J. van Wees, "Electronic spin transport and spin precession in single graphene layers at room temperature," Nature **448**, 571–574 (2007).
[4]M. Johnson, H. Koo, S. Han, and J. Chang, "Spin injection in indium arsenide," Front. Phys. **3**, 62 (2015).
[5]C. Zhang, H. Yao, Y.-H. Nie, J.-Q. Liang, and P.-B. Niu, "Magnetic field manipulation of spin current in a single-molecule magnet tunnel junction with two-electron Coulomb interaction," AIP Adv. **8**, 045309 (2018).
[6]M. Busl and G. Platero, "Spin-polarized currents in double and triple quantum dots driven by ac magnetic fields," Phys. Rev. B **82**, 205304 (2010).

[7]M. Battiato, K. Carva, and P. M. Oppeneer, "Superdiffusive spin transport as a mechanism of ultrafast demagnetization," Phys. Rev. Lett. **105**, 027203 (2010).
[8]D. Rudolf, C. La-O-Vorakiat, M. Battiato, R. Adam, J. M. Shaw, E. Turgut, P. Maldonado, S. Mathias, P. Grychtol, H. T. Nembach, T. J. Silva, M. Aeschlimann, H. C. Kapteyn, M. M. Murnane, C. M. Schneider, and P. M. Oppeneer, "Ultrafast magnetization enhancement in metallic multilayers driven by superdiffusive spin current," Nat. Commun. **3**, 2029 (2012).
[9]N. Bergeard, M. Hehn, S. Mangin, G. Lengaigne, F. Montaigne, M. L. M. Lalieu, B. Koopmans, and G. Malinowski, "Hot-electron-induced ultrafast demagnetization in Co/Pt multilayers," Phys. Rev. Lett. **117**, 147203 (2016).
[10]D. M. Nenno, B. Rethfeld, and H. C. Schneider, "Particle-in-cell simulation of ultrafast hot-carrier transport in Fe/Au heterostructures," Phys. Rev. B **98**, 224416 (2018).
[11]T. Binder, M. Pfeiffer, and S. Fasoulas, "Validation of grid current simulations using the particle-in-cell method for a miniaturized ion thruster," AIP Conf. Proc. **2132**, 040003 (2019).
[12]J. Briones, H. C. Schneider, and B. Rethfeld, "Monte Carlo simulation of ultrafast nonequilibrium spin and charge transport in iron," J. Phys. Commun. **6**, 035001 (2022).
[13]W. Eckstein, *Computer Simulation of Ion-Solid Interactions* (Springer-Verlag, Berlin, 1991).
[14]A. Haghighat, *Monte Carlo Methods for Particle Transport* (CRC Press, Boca Raton, 2014).
[15]A. Haghighat, *Monte Carlo Methods for Particle Transport* (CRC Press, 2020).
[16]D. Landau and K. Binder, *A Guide to Monte Carlo Simulations in Statistical Physics* (Cambridge University Press, 2005).
[17]K. Huthmacher, A. Herzwurm, M. Gnewuch, K. Ritter, and B. Rethfeld, "Monte Carlo simulation of electron dynamics in liquid water," Physica A **429**, 242–251 (2015).
[18]A. Alekhin, I. Razdolski, N. Ilin, J. P. Meyburg, D. Diesing, V. Roddatis, I. Rungger, M. Stamenova, S. Sanvito, U. Bovensiepen, and A. Melnikov, "Femtosecond spin current pulses generated by the nonthermal spin-dependent Seebeck effect and interacting with ferromagnets in spin valves," Phys. Rev. Lett. **119**, 017202 (2017).
[19]O. Kallenberg, *Foundations of Modern Probability* (Springer, New York, 2002).
[20]D. T. Carl Graham, *Stochastic Simulation and Monte Carlo Methods* (Springer-Verlag, Berlin, 2013).
[21]V. V. Kruglyak, R. J. Hicken, M. Ali, B. J. Hickey, A. T. G. Pym, and B. K. Tanner, "Measurement of hot electron momentum relaxation times in metals by femtosecond ellipsometry," Phys. Rev. B **71**, 233104 (2005).
[22]S. Kaltenborn, Y.-H. Zhu, and H. C. Schneider, "Wave-diffusion theory of spin transport in metals after ultrashort-pulse excitation," Phys. Rev. B **85**, 235101 (2012).
[23]R. Ritchie and J. Ashley, "The interaction of hot electrons with a free electron gas," J. Phys. Chem. Solids **26**, 1689–1694 (1965).
[24]M. Bauer, A. Marienfeld, and M. Aeschlimann, "Hot electron lifetimes in metals probed by time-resolved two-photon photoemission," Prog. Surf. Sci. **90**, 319–376 (2015).
[25]B. Y. Mueller and B. Rethfeld, "Relaxation dynamics in laser-excited metals under nonequilibrium conditions," Phys. Rev. B **87**, 035139 (2013).
[26]A. Eschenlohr, M. Battiato, P. Maldonado, N. Pontius, T. Kachel, K. Holldack, R. Mitzner, A. Föhlisch, P. M. Oppeneer, and C. Stamm, "Ultrafast spin transport as key to femtosecond demagnetization," Nat. Mater. **12**, 332 (2013).
[27]A. R. Khorsand, M. Savoini, A. Kirilyuk, and T. Rasing, "Optical excitation of thin magnetic layers in multilayer structures," Nat. Mater. **13**, 101–102 (2014).
[28]W. S. M. Werner, K. Glantschnig, and C. Ambrosch-Draxl, "Optical constants and inelastic electron-scattering data for 17 elemental metals," J. Phys. Chem. Ref. Data **38**, 1013–1092 (2009).